Electronic and magnetic properties of the ionic Hubbard model on the striped triangular lattice at $\frac{3}{4}$ filling

Jaime Merino,[1] Ross H. McKenzie,[2] and B. J. Powell[2]
[1]*Departamento de Física Teórica de la Materia Condensada, Universidad Autónoma de Madrid, Madrid 28049, Spain*
[2]*Centre for Organic Photonics and Electronics, School of Mathematics and Physics, The University of Queensland, Brisbane 4072, Australia*

(Received 23 April 2009; revised manuscript received 25 June 2009; published 20 July 2009)

We report a detailed study of a model Hamiltonian which exhibits a rich interplay of geometrical spin frustration, strong electronic correlations, and charge ordering. The character of the insulating phase depends on the magnitude of the onsite energy $\Delta/|t|$ and on the sign of the hopping amplitude t. We find a Mott insulator for $\Delta \gg U \gg |t|$; a charge-transfer insulator for $U \gg \Delta \gg |t|$; and a correlated covalent insulator for $U \gg \Delta \sim |t|$, with U the onsite Coulomb repulsion energy. The charge-transfer insulating state is investigated using a strong-coupling expansion. The frustration of the triangular lattice can lead to antiferromagnetism or ferromagnetism depending on the sign of t. We identify the "ring" exchange process around a triangular plaquette which determines the sign of the magnetic interactions. Exact diagonalization calculations are performed on the model for a wide range of parameters and compared to the strong-coupling expansion. The regime $U \gg \Delta \sim |t|$ and $t<0$ is relevant to $Na_{0.5}CoO_2$. The calculated optical conductivity and the spectral density are discussed in the light of recent experiments on $Na_{0.5}CoO_2$.

DOI: 10.1103/PhysRevB.80.045116 PACS number(s): 71.10.Fd, 71.15.−m, 71.27.+a

I. INTRODUCTION

Many strongly correlated electron materials exhibit a subtle competition between different magnetic and charge ordered states, and between metallic, insulating, and superconducting phases. Widely studied (and poorly understood) materials include cuprate superconductors,[1] organic charge-transfer salts,[2] manganites with colossal magnetoresistance,[3] heavy fermion compounds,[4] and the iron pnicitide superconductors.[5] A fundamental theoretical challenge is explaining the hierarchy of energy scales and competing phases in these materials. The energy scales (such as the bandwidth and Coulomb repulsion) associated with the relevant electronic orbitals (and microscopic Hamiltonians such as Hubbard models) are typically on the order of eV. In contrast, the energy scales associated with the temperature and magnetic field dependences of transport properties and energy differences between competing phases are often several orders of magnitude smaller. Frustration of spin or charge ordering by competing interactions due to the geometry of the crystal lattice can enhance these effects. In addition, it is not clear what physical changes are produced by chemical doping. For example, does adding charge carriers just change the band filling or are there significant effects due to the associated disorder and changes in the electronic structure?

Here we report a detailed study of a specific strongly correlated electron model, the ionic Hubbard model on the triangular lattice at 3/4 filling with a stripe potential. The model illustrates how the interplay of geometric frustration and strong correlations lead to competition between different magnetic orders, charge ordering, metallic, and insulating behaviors. One concrete realization of the model is that it may be the simplest many-body Hamiltonian that can describe $Na_{0.5}CoO_2$.[6–8] Elsewhere we have reviewed experimental results on this material and described recent theoretical attempts to describe its unusual properties.[8] When the filling x in Na_xCoO_2 is close to other commensurate values, such as 1/3, 2/3, or 3/4, the system is still described by an ionic Hubbard model but the on-site potential has a different form and commensurability, depending on the ordering arrangement of the sodium ions.[6] At $x=4/5$, such a model[9] has been suggested to be relevant to the ordering observed in $Na_{0.8}CoO_2$. At incommensurate values of x one expects phase coexistence of multiple Na-ordering phases.[10]

The rest of the paper is organized as follows: in Sec. II we introduce an ionic Hubbard model on a triangular lattice including a discussion of its phase diagram. In Sec. III we analyze the model's ground-state properties using the Lanczos exact diagonalization technique on finite-size clusters. Dynamical properties such as the spectral density and optical conductivity are discussed in Sec. IV. Finally, a summary of the main results and their relevance to $Na_{0.5}CoO_2$ is given in Sec. V. We have also studied the same model using a complementary method, mean-field slave bosons.[8] At appropriate places in the paper we compare and contrast the results.

II. IONIC HUBBARD MODEL ON A TRIANGULAR LATTICE

The Hamiltonian of the ionic Hubbard model is

$$H = -t \sum_{\langle ij \rangle \sigma} (c^+_{i\sigma} c_{j\sigma} + c^+_{j\sigma} c_{i\sigma}) + U \sum_i n_{i\uparrow} n_{i\downarrow} + \sum_{i\sigma} \epsilon_i n_{i\sigma}, \quad (1)$$

where $c^+_{i\sigma}$ creates an electron with spin σ at site i, t is the hopping amplitude between neighboring sites, and U is the effective on-site Coulomb repulsion energy between two electrons. We set $\epsilon_i = \Delta/2$ for the A sites and $\epsilon_i = -\Delta/2$ for B sites (cf. Figure 1). The A sites form rows which alternate with the B sites of the triangular lattice. By a particle-hole transformation: $c^+_{i\sigma} \rightarrow h_{i\sigma}$ model (1) becomes a 1/4-filled

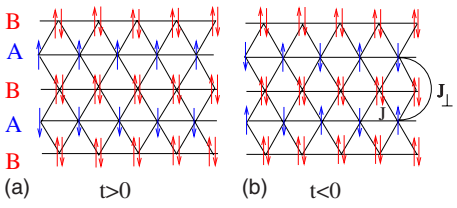

FIG. 1. (Color online) Spin and charge order in the 3/4-filled Ionic Hubbard model (1) on a triangular lattice in the limit $U \gg \Delta \gg |t|$. A and B denote the inequivalent sites of the lattice. C-type antiferromagnetism (left) is found for $t>0$ in contrast to G-type antiferromagnetism (right) for $t<0$. The exchange couplings J and $J_\perp$ are defined in Eq. (7) for the appropriate $t-J$ model in Eq. (6). A ferromagnetic exchange coupling, J, between neighboring A sites occurs for the parameter range: $0<5t<\Delta<\sqrt{2}U$.

(with holes) ionic Hubbard model with the sign transformation: $t \to -t$ and $\Delta \to -\Delta$.

In what follows we will discuss the charge gap which is defined for the model on a finite lattice with N electrons and $2N/3$ lattice sites by

$$\Delta_c \equiv E_0(N+1) + E_0(N-1) - 2E_0(N), \tag{2}$$

where $E_0(M)$ is the ground-state energy of the system with M electrons.

A. Previous theories of the ionic Hubbard model

The ionic Hubbard model (1) on the striped triangular lattice of Fig. 1 considered here contains geometrical frustration. This is in contrast to most previous work which has focused on bipartite, i.e., unfrustrated, lattices with different site energies, Δ, on each of the bipartite sublattices and at half-filling. Some of the interest in this model can be appreciated from the half-filled atomic limit ($t=0$). For $U>\Delta$ the charge gap for the addition of particles defined in Eq. (2), $\Delta_c = U-\Delta$; thus, the system is a Mott insulator. But, for $U<\Delta$, $\Delta_c = \Delta - U$; and the system is a band insulator. At the point $U=\Delta$ this gap vanishes. Therefore a key question is what happens at the band to Mott insulator transition away from the atomic limit; in particular what happens to the gapless point—does it expand give a metallic phase? Further impetus comes from the proposals that the ionic Hubbard model is important for understanding ferroelectric perovskites,[11] organic charge-transfer salts,[12,13] transition-metal oxide heterostructures,[14] and nonlinear electronic polarizability in transition-metal oxides,[15] and, as discussed below the rich electronic phases observed in A_xCoO_2 [A=Na, K, Rb].[8]

The most studied case is the half-filled one-dimensional (1D) chain with different site energies for odd and even numbered sites. This model shows three distinct insulating phases: a band insulator, a (ferroelectric) bond order wave insulator, and a Mott insulator.[16] Metallic behavior appears to be limited to the point in the phase diagram where band insulator gives way to the bond order wave insulator.[16] Continuum limit bosonization calculations suggest that adding a next-nearest-neighbor hopping, t', (which is equivalent to studying the zigzag chain) induces a large metallic region in the phase diagram,[17] suggesting that even in one-dimension frustration already plays an important role in the ionic Hubbard model.

The infinite-dimensional ionic Hubbard model has been studied using dynamical mean-field theory (DMFT),[18,19] which treats the on-site quantum dynamics exactly but ignores spatial correlations such as those associated with antiferromagnetic exchange. These papers studied the bipartite Bethe lattice and found that a metallic phase separates the band insulating phase from the Mott insulating phases, in, at least, some parts of the phase diagram.

In two dimensions most previous work has focused on the half-filled square lattice with site energies alternating in a checkerboard pattern. This model has been studied using both cluster DMFT[20] and determinant quantum Monte Carlo (DQMC).[21,22] These studies all suggested that a phase with nonzero spectral weight at the Fermi energy exists between the band insulator and Mott insulator phases, at least in some of the phase diagram. However, there has been some debate over whether this phase is metallic[21,22] or bond ordered.[20]

There has been far less work on the ionic Hubbard model away from half-filling. However, Penc *et al.*[23] studied the quarter-filled ionic Hubbard model on the zigzag ladder and found a competition between ferromagnetism and a paramagnetic phase with strong antiferromagnetic correlations. Bouadim *et al.*[22] studied the ionic Hubbard model on a square lattice with a checkerboard potential across all possible fillings with DQMC. The most interesting features they found, away from half filling, were Mott insulation at quarter and three quarters filling (which are related by the particle-hole symmetry of this model). Bouadim *et al.* did not find any evidence of magnetic order in this phase. However, as the magnetic interactions are $\mathcal{O}(t^4/U\Delta^2)$ the absence of magnetic order may be due to nonzero value of the temperatures they studied.

As well as bipartite arrangements of the different site energies there has also been considerable interest in random arrangements of site energies. Laad *et al.*[24] studied a system with a Gaussian density of states and a bimodal distribution of site energies in infinite dimensions for various impurity concentrations, n, and fillings, $1-\delta$. They found insulating states for $\delta = 1-n$ and sufficiently large Δ and U. Byczuk *et al.* have used DMFT to study the (frustrated) fcc[26] and (bipartite) Bethe[25] lattices in infinite dimensions with a bimodal distribution of site energies and half the sites taking each value of the site energy. At one-quarter filling they found that metal-insulator transitions occur on both lattices when both U and Δ are sufficiently large. They also noted that DMFT does not capture some of the possible effects of the disorder, such as Anderson insulating phases. In two dimensions Paris *et al.*[21] used DQMC to study the square lattice at a range of fillings with 1/8 of the sites randomly chosen to have a different site energy than the rest of the lattice. They found that this model displayed Mott insulating, band insulating, Anderson insulating, and metallic phases.

Marianetti and Kotliar[27] simplified our suggestion[6] of that Eq. (1) is the appropriate effective low Hamiltonian for Na_xCoO_2 by further assuming that Na-ordering is of secondary importance and hence treated the potential due to the Na ions as random. They then used density functional theory to

show that the distribution of Co site energies is bimodal and to parameterize the Hamiltonain (1) for $x=0.3$ and 0.7. Finally they calculated the high-temperature ($T \gtrsim 100$ K) susceptibility for these dopings and found them to be in qualitative agreement with experiment. We deal here with the case $x=0.5$ for which Na-ordering of the stripe-type (cf. Fig. 1) has been observed in experiments.[28,29]

B. Noninteracting model ($U=0$)

For $U=0$ model (1) can be diagonalized straightforwardly leading to two bands, denoted $\pm$. We introduce creation and destruction operators

$$c^{\dagger}_{\mathbf{k}\pm\sigma} = \alpha_{\mathbf{k}\mp}(c^{+}_{A\mathbf{k}\sigma} + A_{\mathbf{k}\mp}c^{+}_{B\mathbf{k}\sigma}), \tag{3}$$

where $c^{+}_{A\mathbf{k}\sigma}$ and $c^{+}_{B\mathbf{k}\sigma}$ act on the Bloch states associated with the A and B sublattices, respectively, and

$$A_{\mathbf{k}\pm} = \frac{\Delta/2 \pm \sqrt{\Delta^2/4 + [4t\cos(k_x/2)\cos(k_y\sqrt{3}/2)]^2}}{4t\cos(k_x/2)\cos(k_y\sqrt{3}/2)}, \tag{4}$$

with the normalization constant $\alpha_{\mathbf{k}\pm} = 1/\sqrt{1+|A_{\mathbf{k}\pm}|^2}$. The energy dispersion of the two bands is

$$\epsilon_{\pm}(\mathbf{k}) = -2t\cos k_x \pm \sqrt{\Delta^2/4 + [4t\cos(k_x/2)\cos(k_y\sqrt{3}/2)]^2}, \tag{5}$$

with k_x and k_y defined in the reduced $(1\times\sqrt{3})$ Brillouin zone with lattice-parameter $a=1$. At 3/4-filling and for any Δ, there is always at least one band crossing the Fermi energy and so the system is metallic. The + band is half-filled and the − band filled for $t>0$ and $\Delta>0$, whereas for $t<0$ this only occurs for $\Delta > 0.64|t|$. For $\Delta=0$ there is only one band, which has a width of $W=9|t|$.

C. Phase diagram

The ionic Hubbard model (1) on a triangular lattice contains a rich phase diagram resulting from the interplay between geometrical frustration, strong Coulomb repulsion, and charge ordering phenomena. A schematic phase diagram can be constructed by first considering some simple limits:

(i) $t=0$ (atomic limit): all A sites are singly occupied while B sites are doubly occupied. The system is insulating with a charge gap: $\Delta_c = \min(\Delta, U)$. For $\Delta > U$ it is a Mott insulator (MI) with $\Delta_c = U$, whereas for $\Delta < U$ it is a charge-transfer insulator (CTI) with $\Delta_c = \Delta$.

(ii) $U=0$ (noninteracting limit): as discussed above the model is always metallic regardless the value of Δ.

(iii) $\Delta=0$: for any U the model reduces to the regular Hubbard model on the isotropic triangular lattice at 3/4-filling. For large $U/|t|$, it is equivalent to the $t-J$ model on the triangular lattice. Dynamical mean-field theory calculations[6,30] give a ground state that is metallic. DMFT[6] calculations on the Hubbard model for large U and variational Monte Carlo calculations on the $t-J$ model give this metallic ground state as paramagnetic (ferromagnetic) for $t<0 (t>0)$.[31]

(iv) $\Delta=\infty$: as the B sites can be completely projected out from the Hilbert space, the model is mapped onto decoupled half-filled Hubbard chains. Hence, the system is (Mott) insulating for any nonzero positive U; i.e., there is a charge gap $\Delta_c \neq 0$, and there are antiferromagnetic correlations (with power-law decay) and no spin gap.

(v) $U \gg \Delta \gg |t| \neq 0$: for finite but small t, virtual hopping processes lead to effective magnetic exchange couplings between the A sites. The effective low-energy $t-J-J_{\mathrm{diag}}-J_{\perp}$ Hamiltonian for the holes is

$$H = t\sum_{ij\sigma} P(h^{+}_{i\sigma}h_{j\sigma} + h^{+}_{j\sigma}h_{i\sigma})P + J\sum_{\{ij\}}\left[\mathbf{S_i}\cdot\mathbf{S_j} - \frac{n_i n_j}{4}\right] + J_{\mathrm{diag}}\sum_{(ij)}\left[\mathbf{S_i}\cdot\mathbf{S_j} - \frac{n_i n_j}{4}\right] + J_{\perp}\sum_{[ij]}\left[\mathbf{S_i}\cdot\mathbf{S_j} - \frac{n_i n_j}{4}\right] - \sum_{i\sigma}\epsilon_i h^{+}_{i\sigma}h_{i\sigma}, \tag{6}$$

where $\{\ldots\}$ and $[\ldots]$ denote sums over intra-A-chain, inter-A-chain sites, respectively. The sum over $(\ldots)$ is between an A and nearest-neighbor B sites. The projector $P=\Pi_i[1-n_{i\uparrow}n_{i\downarrow}]$ forbids double occupation of holes on any lattice site. The dynamics of the electron-doped system relevant to Na_xCoO_2 with electron occupation $1+x$ is related to the hole-doped system, with filling $1-x$, through the replacement: $t\to -t$ and $\epsilon_i \to -\epsilon_i$ leaving the exchange parameters unchanged.

The exchange couplings J, $J_{\perp}$, and J_{diag} can be obtained through a strong-coupling expansion using Raleygh-Schrödinger perturbation theory on the hopping term around the configuration in which all B sites are doubly occupied and A sites singly occupied (see Appendix A). This leads to an effective exchange coupling between electrons in A sites in the horizontal direction

$$J = \frac{4t^2}{U} - \frac{8t^3}{\Delta^2} - \frac{16t^3}{\Delta U} + \mathcal{O}(t^4), \tag{7}$$

and in the perpendicular direction

$$J_{\perp} = \frac{16t^4}{\Delta^2}\left[\frac{1}{U} + \frac{1}{2\Delta+U} + \frac{1}{2\Delta}\right] + \mathcal{O}(t^5). \tag{8}$$

The exchange coupling J_{diag} between A and B sites is

$$J_{\mathrm{diag}} = 2t^2\left[\frac{1}{U+\Delta} + \frac{1}{U-\Delta}\right] + \mathcal{O}(t^3), \tag{9}$$

which is blocked if the B sites are doubly occupied but recovers the correct $4t^2/U$ exchange interaction as $\Delta \to 0$.

The second and third terms in J are antiferromagnetic (AFM) for $t<0$ and ferromagnetic (FM) for $t>0$. Higher-order contributions to J are AF and can be found in Appendix A.

A schematic phase diagram of the 3/4-filled ionic Hubbard model on a triangular lattice (1) is shown in Fig. 2. The transition lines are extracted from the limits (i)-(v) discussed above and exact diagonalization calculations for intermediate parameter regimes. Apart from the Mott insulator and charge-transfer insulator, our numerical analysis suggests the presence of a covalent insulator (CI) in the range $\Delta \sim \mathrm{O}(|t|)$ and $U \gg |t|$. Depending on the sign of t, different spin ar-

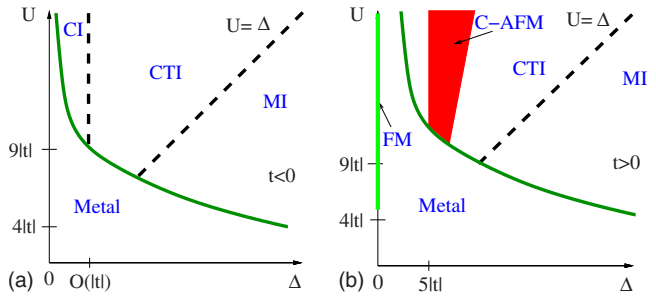

FIG. 2. (Color online) Schematic phase diagram of the Ionic Hubbard model 1 on a striped triangular lattice at 3/4-filling. The transition lines are based on the lowest-order corrections in a strong-coupling analysis and on Lanczos diagonalization calculations. The $t<0$ case is relevant to the $Na_{0.5}CoO_2$ insulator. Insulating phases at strong-coupling, $U>W$, of different types are found ranging from a charge-transfer insulator (CTI), a Mott Insulator (MI), and a covalent insulator (CI). The bandwidth of the model for $\Delta=0$ (the isotropic triangular lattice), $W=9|t|$, is effectively reduced to $4|t|$ corresponding to one-dimensional (1D) chains as Δ increases. At exactly $\Delta=\infty$, the system is insulating for any nonzero U as expected for a half-filled Hubbard chain due to Umklapp processes. The blue line is an estimate of the critical U for the metal-to-insulator transition which follows the effective bandwidth dependence with Δ. Insulating phases for $t<0$ display G-type antiferromagnetic (AFM) (see Fig. 1) correlations whereas a C-AFM region (see Fig. 1) for $t>0$ is obtained from the condition, $J<0$, to Eq. (7) which we assume valid for $U\gtrsim 9|t|$. The marked $\Delta=0$ axis for $t>0$ and above $U\approx 5|t|$ indicates the occurrence of ferromagnetism as predicted by DMFT of the Hubbard model on an isotropic triangular lattice. (Ref. 6)

rangements occur as shown in Fig. 1. The condition $J=0$ separates AF from the FM region which occurs in the parameter range: $5t<\Delta<\sqrt{2U}$ and is plotted in Fig. 2.

D. Model on two- and four-site clusters

In this section we explore the nature of the ground state of the model (1) on two- and four-site clusters. The two-site cluster incorporates charge ordering phenomena in the presence of on-site Coulomb interaction. The four-site toy model also contains geometrical frustration effects present in the full model (1). Ground-state properties of the clusters are discussed in terms of valence-bond (VB) theory[32] when appropriate. For $t<0$ and $U\gg|t|$ the ground-state wave function is accurately described by the resonance between possible valence bonds. Our analysis indicates that the charge gap of the clusters is enhanced with Δ due to the differences between the two-electron and three-electron bonds between the different A and B sites.

1. Two-site cluster

We first consider three electrons in two inequivalent sites (one A, the other B) separated by an energy Δ. The energy levels for this cluster are sketched in Fig. 3. The Hamiltonian is

$$H=-t(c^{+}_{A\sigma}c_{B\sigma}+c^{+}_{B\sigma}c_{A\sigma})+U(n_{A\uparrow}n_{A\downarrow}+n_{B\uparrow}n_{B\downarrow}) + \Delta/2(n_A-n_B). \quad (10)$$

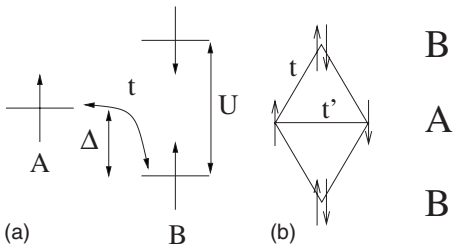

FIG. 3. Ionic Hubbard model on two- and four-site clusters. The energy-level diagram for three electrons on two sites (left) and the four-site cluster with six electrons (right).

For $U=0$, the charge gap of the cluster is $\Delta_c=0$ for any Δ due to the degeneracy of the ground state. In order to evaluate the dependence of the gap on Δ we first obtain the ground-state energies with $N=2$, 3, and 4 electrons

$$E_0(2)=-2t^2\left[\frac{1}{U+\Delta}+\frac{1}{U-\Delta}\right], \quad U\gg|t|$$

$$E_0(3)=U-\frac{\sqrt{\Delta^2+4t^2}}{2}$$

$$E_0(4)=2U. \quad (11)$$

In the limit $\Delta\to 0$ and $U\gg|t|$, the charge gap of the cluster is

$$\Delta_c\approx 2|t|+\Delta^2\left(\frac{1}{4t}-\frac{4t^2}{U^3}\right)-\frac{4t^2}{U}. \quad (12)$$

The first contribution to Δ_c is present even for $\Delta=0$ as expected from the bonding-antibonding splitting of the cluster and will go to zero in the infinite system. The term proportional to Δ^2 comes from the different dependances of $E(3)$ and $E(2)$ on Δ: $E(2)$ has a weaker dependence than $E(3)$. This is due to the different nature of the two-electron and the three-electron bond. The former is accurately described by a correlated VB between an electron on an A site and an electron on a B site whereas the latter is described by a single hole in an antibonding "molecular" orbital. The two-electron and three-electron bond energies (the energy needed to break a bond between inequivalent sites) are $\Delta/2-\sqrt{\Delta^2+4t^2}/2$ and $E_0(2)$, respectively. Hence, the two-electron bond becomes weaker with Δ while the three-electron bond is strengthened with Δ. This is known from quantum chemistry[32] and can be understood as being a consequence of the presence or absence of Coulomb repulsion between electrons.

2. Four-site cluster

We consider the four-site cluster (Fig. 3) with two A sites shifted by $+\Delta/2$ and two B sites shifted by $-\Delta/2$. The cluster shown contains $N=6$ electrons (corresponding to 3/4-filling). The model Hamiltonian in this case is

$$H=-t\sum_{i\in A,j\in B}(c^{+}_{i\sigma}c_{j\sigma}+c^{+}_{j\sigma}c_{i\sigma})-t'\sum_{i,j\in A}(c^{+}_{i\sigma}c_{j\sigma}+c^{+}_{j\sigma}c_{i\sigma}) + U\sum_i n_{i\uparrow}n_{i\downarrow}+\Delta/2\sum_{i\in A,j\in B}(n_i-n_j). \quad (13)$$

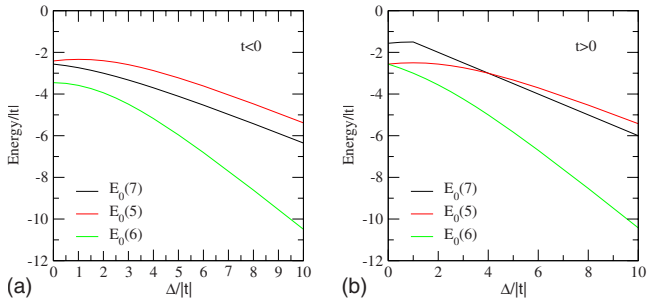

FIG. 4. (Color online) Dependence of ground-state energies with Δ for the four-site cluster with $t'=t$ and $U=100|t|$. The Coulomb interaction U, $2U$, and $3U$ have been subtracted from the total energies $E_0(5)$, $E_0(6)$, and $E_0(7)$, respectively, for convenience.

We first discuss the $\Delta \to 0$ limit. The exact ground-state energies of the fully frustrated $t'=t$ cluster for $N=5$, 6, and 7 electrons are plotted in Fig. 4 for $U=100|t|$. Consistent with the results for the two-site cluster we find that, $E_0(5)$, has the weakest dependence on Δ of all the ground-state energies. The ground-state wave function for $N=6$ can be well described in terms of resonating valence bonds as shown in the Appendix B. In contrast, the wave function for $N=7$ consists of a single-hole hopping around the cluster and so contains no Coulomb interaction effects. In this case a "molecular" orbital with a single hole describes the cluster and its energy, $E_0(7)$, has the strongest dependence with Δ. The different behavior of $E_0(N)$, $E_0(N+1)$, and $E_0(N-1)$ is responsible for the increase in the charge gap with Δ as shown in Fig. 5. This behavior is in contrast to the $U=0$ case plotted in the figure.

Effects of frustration. We now discuss the four-site cluster with $t'=0$. In this case analytical formulas may be obtained for $U=\infty$. The sign of the hopping is irrelevant here in contrast to the $t' \neq t$ case. The ground-state energies are

$$E_0(6) = -\sqrt{8t^2 + \Delta^2}$$

$$E_0(7) = -t - \frac{\sqrt{4t^2 + \Delta^2}}{2}. \tag{14}$$

In the limit $\Delta \to 0$, we find $E_0(7) \approx -2t - \frac{\Delta^2}{4|t|}$ and $E_0(6) \approx -2\sqrt{2}t - \frac{\sqrt{2}\Delta^2}{8|t|}$. Thus, $E_0(6)$ has a weaker dependence

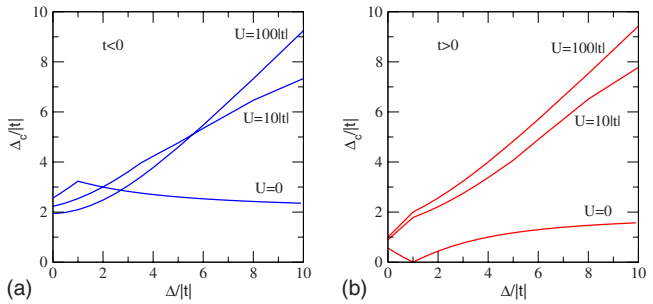

FIG. 5. (Color online) Dependence of the charge gap on Δ for the four-site cluster. Note the increase of Δ_c for any Δ for $U \gg |t|$ of Fig. 4 and also how the dependence for $\Delta > |t|$ is quite different with $\Delta < |t|$.

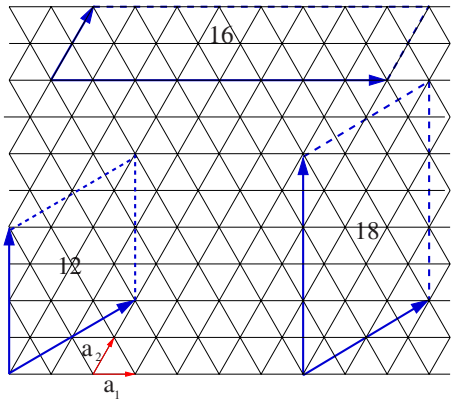

FIG. 6. (Color online) Cluster shapes of different sizes used in exact diagonalization calculations.

on Δ than $E_0(7)$, similarly to the fully frustrated $t'=t$ cluster.

Our small cluster analysis indicates that the charge gap, Δ_c, increases with Δ due to the different natures of the two-electron and three-electron bonds formed between inequivalent sites. This result is not affected by the presence of frustration in the cluster at the qualitative level. However, geometrical frustration ($t \sim t'$) leads to qualitatively different magnetic properties for different signs of t in contrast to the unfrustrated ($t'=0$) case.

III. GROUND-STATE PROPERTIES OF THE IONIC HUBBARD MODEL ON A TRIANGULAR LATTICE

Intermediate parameter regimes are explored based on Lanczos diagonalization on finite clusters with $N_s=12$, 16, and 18 sites and periodic boundary conditions. Different cluster shapes have been benchmarked against the exact solution of the noninteracting model (1) and are shown in Fig. 6. The vectors defining the clusters are: $\mathbf{T}_1 = n_{11}\mathbf{a}_1 + n_{12}\mathbf{a}_2$ and $\mathbf{T}_2 = n_{21}\mathbf{a}_1 + n_{22}\mathbf{a}_2$, where n_{1i} and n_{2i} are integers. A straightforward finite-size scaling analysis is not possible because of the complicated changes in the cluster shape as the lattice size increases.

We present results of the dependence of the charge order parameter, the charge gap, and the spin correlations on Δ. Numerical results are compared to the weak and strong-coupling limits as appropriate.

A. Charge order

The charge order parameter is first computed for $U=0$ and compared to exact tight-binding results on the infinite lattice. This serves to calibrate the importance of finite-size effects on a cluster. Second, the effect of U on charge ordering is analyzed in detail.

The charge order parameter is

$$n_B - n_A = \sum_{\mathbf{k},\sigma} \langle \Psi_0 | (c^\dagger_{B\mathbf{k}\sigma} c_{B\mathbf{k}\sigma} - c^\dagger_{A\mathbf{k}\sigma} c_{A\mathbf{k}\sigma}) | \Psi_0 \rangle, \tag{15}$$

where $|\Psi_0\rangle$ is the ground state of the Hamiltonian (1).

In Fig. 7 the charge order parameter is plotted for both signs of t on the $N_s=18$ site cluster of Fig. 6 and compared to

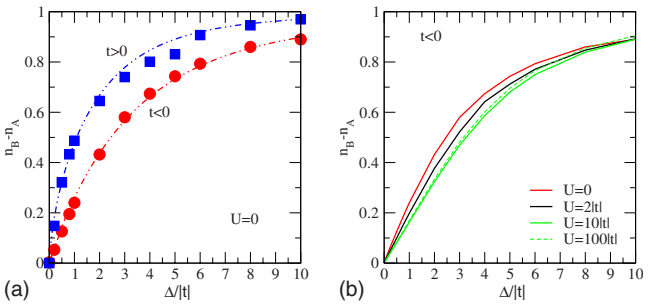

FIG. 7. (Color online) Charge disproportionation, $n_B - n_A$, between inequivalent rows in the ionic Hubbard model 1. In (a) tight-binding (dash-dotted lines) exact results for $U=0$ are compared with Lanczos diagonalization (closed symbols) for the $N_s=18$ tilted cluster of Fig. 6 showing good agreement. In (b) the dependence of $n_B - n_A$ with U is shown from Lanczos diagonalization for $t<0$ on the same cluster.

the tight-binding result ($U=0$) of the extended system. Since this cluster gives the best agreement with the infinite limit of the noninteracting model, among all of the clusters that we studied, we mostly show results for this cluster in the rest of this paper.

The effect of Coulomb repulsion on charge transfer is also shown in Fig. 7. The qualitative dependence of charge transfer remains unchanged with U. However, increasing U does suppress $n_B - n_A$ a little for small and moderate Δ.

In $Na_{0.5}CoO_2$ the strong Coulomb interaction and weak charge transfer imply:[7,8] $U \gg \Delta$ and $\Delta \sim |t|$. Note also that in this parameter regime charge transfer between A and B sites is weak: $n_B - n_A < 0.2$, for $\Delta \sim |t|$ which implies that a charge-transfer insulator formed by doubly occupied B sites alternating with half-filled A sites is not possible.

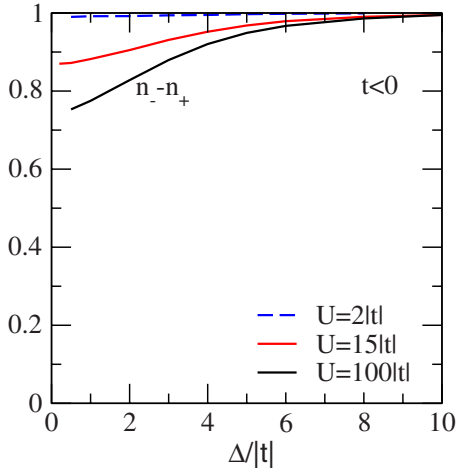

FIG. 8. (Color online) Difference in filling of the hybrid ± bands as a function of $\Delta/|t|$ for $t<0$ and several values of $U/|t|$. Results are from Lanczos calculations on 18-site clusters.

B. Reciprocal space-charge ordering

We now turn our attention to the charge populations of the one-electron (−) and (+) hybrid bands obtained in Eq. (5) for $U=0$. The upper (lower) tight-binding band is half-filled (filled) for any nonzero Δ in the $t>0$ case[8] while for $t<0$ this is only the case for: $\Delta > 0.68|t|$. Simple arguments might then suggest that if U is sufficiently large then the half-filled band may undergo a Mott insulator transition. However, for such a single-band argument to be valid the half-filled + band must be sufficiently high in energy above the filled band so that interband transitions induced by U can be safely neglected.

In the basis of the noninteracting +,− band states the Hamiltonian is

$$H = \sum_{\mathbf{k}\alpha,\sigma} \epsilon_\alpha(\mathbf{k}) c^+_{\mathbf{k}\alpha,\sigma} c_{\mathbf{k}\alpha,\sigma} + \frac{1}{N_s} \sum_{\mathbf{k},\mathbf{k}',\mathbf{q}\alpha_1,\alpha_2,\alpha_3,\alpha_4} V(\mathbf{k}-\mathbf{q}\alpha_1, \mathbf{k}\alpha_2, \mathbf{k}'+\mathbf{q}\alpha_3, \mathbf{k}'\alpha_4) c^+_{\mathbf{k}-\mathbf{q}\alpha_1,\sigma_1} c^+_{\mathbf{k}'+\mathbf{q}\alpha_3,\sigma_2} c_{\mathbf{k}'\alpha_4,\sigma_2} c_{\mathbf{k}\alpha_2,\sigma_1}, \quad (16)$$

where the α's refer to the two values + and − and V is the Coulomb matrix describing the 16 different scattering processes between the bands: $\epsilon_\alpha(\mathbf{k})$ of Eq. (5). The Coulomb matrix is

$$V(\mathbf{k_1}\alpha_1, \mathbf{k_2}\alpha_2, \mathbf{k_3}\alpha_3, \mathbf{k_4}\alpha_4) = U\beta(\mathbf{k_1}\alpha_1)\beta^*(\mathbf{k_2}\alpha_2)\beta(\mathbf{k_3}\alpha_3)\beta^*(\mathbf{k_4}\alpha_4), \quad (17)$$

with

$$\beta(\mathbf{k}\pm) = \frac{1}{\alpha_{\mp\mathbf{k}}} \frac{A_{\mathbf{k}\pm}}{A_{\mathbf{k}\pm} - A_{\mathbf{k}\mp}}, \quad (18)$$

where $A_{\mathbf{k}\pm}$ is given by (4) and $\alpha_\mathbf{k}$, the normalization constant of Eq. (3).

The occupation of the noninteracting bands is obtained through the expression: $n_\pm = \Sigma_{\mathbf{k}\sigma} \langle \Psi_0 | c^+_{\mathbf{k}\pm\sigma} c_{\mathbf{k}\pm\sigma} | \Psi_0 \rangle$.

In order to investigate the populations of the noninteracting bands at large U we plot Lanczos results for $n_- - n_+$ for $N_s=18$ in Fig. 8. For $U=2|t|$, we find that $n_- - n_+ = 1$. However, $n_- - n_+ < 1$ for large U. The interpretation of this result is complicated as $n_- - n_+$ conflates two effects: (i) charge transfer between the bands, effectively doping the + band with electrons from the lower band; and (ii) for $U \neq 0$ the bands are no longer eigenstates, thus the physical interpretation of $n_- - n_+$ is unclear for large U. In spite of this interpretative difficulties it is interesting to note that the behavior seen in Fig. 8 differs from a recent mean-field approach[8] which includes local electron correlations only. However, at present, it is not possible to conclusively determine whether

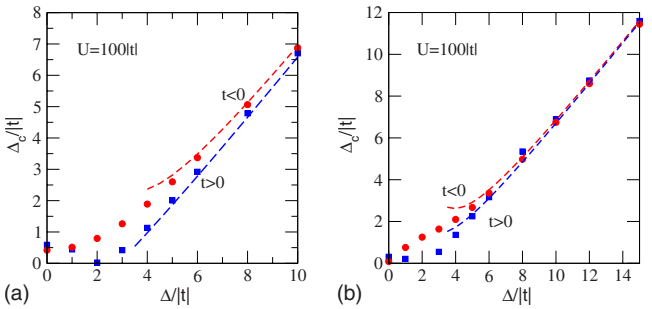

FIG. 9. (Color online) Dependence of the charge gap on the on-site potential Δ. The charge gap for $U=100|t|$ on a $N_s=18$ tilted cluster (a) and a $N_s=16$ ladder-type cluster (b) (see Fig. 6) is shown. Dashed lines denote the results of the strong-coupling expansion (19) for comparison.

this is because nonlocal electron correlations may play an important role or because of the strong interband scattering induced by the large U which will eventually destroy the reciprocal space description. This question is particularly important given the proposed role of tiny hole densities in the + band[8] in explaining the apparent discrepancy between the insulating behavior suggested by resistivity,[28,34] angular resolved photoemission spectra (ARPES),[35] and optical conductivity[43] and the observation of metallic quasiparticles via Shubnikov–de Haas experiments[34] on $Na_{0.5}CoO_2$. This question requires future investigation.

C. Charge gap

In order to understand the electronic properties of model (1) we now discuss the charge gap and its dependence with charge order driven by Δ and the Coulomb repulsion. The charge gap is defined by Eq. (2). When t is small, the lowest-order correction to excitation energies come from the kinetic energy gain due to the propagation along the $B(A)$ chains of a hole (doublon) when extracting (adding) an electron to the zeroth-order ground-state configuration. Using degenerate perturbation theory on Hamiltonian (6) the gap to $O(t^2/\Delta)$ is

$$\Delta_c = \Delta - 2|t| + 8t^2/\Delta - 2t_{\rm eff}^{(2)} - 8t^3/\Delta^2 + \delta E_{1D}^{t-J}, \qquad (19)$$

where δE_{1D}^{t-J} is the energy change when adding a hole to a single half-filled A chain modeled by the $t-J$ model with J given by Eq. (7). The second-order hopping term $t_{\rm eff}^{(2)}=2t^2/\Delta$, contributes to the propagation of an antiholon in the A chain. In the antiferromagnetic case, $J>0$, the energy, δE_{1D}^{t-J} in (19) per A chain site is given by the Bethe ansatz expression[33]

$$\delta E_{1D}^{t-J} = \frac{-2|t|}{\pi}\sin(n_A\pi) - 8J(\ln 2)n_A^2\left[\frac{1-\sin(2n_A\pi)}{2n_A\pi}\right] + J\ln 2, \qquad (20)$$

where $n_A=1-1/N_C^A$ is the number of electrons in a single A chain of N_C^A sites when a single hole has been added to the otherwise half-filled chain. In the ferromagnetic case ($J<0$)

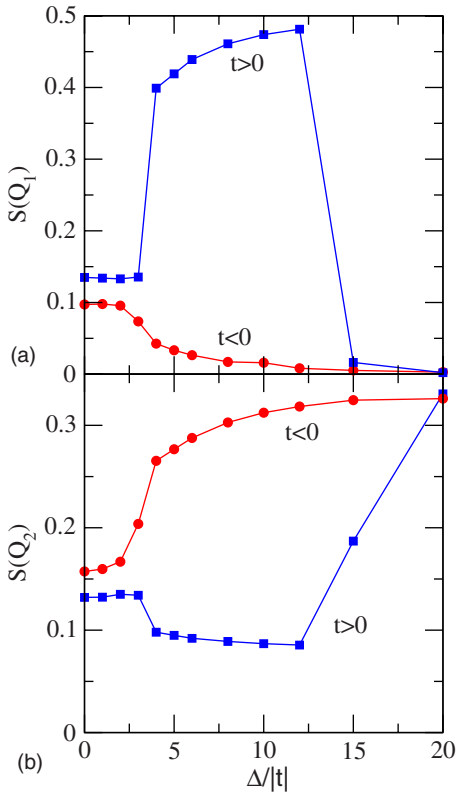

FIG. 10. (Color online) Development of magnetic order. The static spin structure factor $S(\vec{q})$ at the wavevectors (a) $\mathbf{Q}_1=(0,\pi/\sqrt{3})$, associated with C-type antiferromagnetism (Ref. 36) (see Fig. 1, left panel), and (b) $\mathbf{Q}_2=(\pi,\pi/\sqrt{3})$, associated with G-type antiferromagnetism (Ref. 36) (see Fig. 1, right panel), are shown for $U=100|t|$ as a function of Δ, the difference between the local energies on the A and B sublattices. Calculations are performed on the $N_s=18$ cluster.

$$E_{1D}^{t-J} = -2|t| - J/2. \qquad (21)$$

Hence, the charge gap is found to be larger for $t<0$ than $t>0$, as shown in Fig. 9, due to the geometrical frustration. In contrast, on the square lattice, Δ_c, does not depend on the sign of t. The dependence on the sign of t becomes even more apparent for $\Delta\sim|t|$, where it is clear that for $t<0$ the gap is significantly larger than for $t>0$. Indeed, it may be that for small $\Delta/|t|$ and $t<0$ the system is an insulator and for $t>0$ it is metallic. However, finite-size effects prevent us from making a definitive statement about the existence of a metallic state for small $\Delta/|t|$. We note that dependence on the sign of t is the opposite from what one would expect from weak-coupling arguments. For $t>0$ and $U=\Delta=0$ and at 3/4-filling the Fermi surface has perfect nesting and there is a van Hove singularity in the density of states at the Fermi energy. Hence, weak-coupling arguments would suggest that for this sign of t the system would have a greater tendency to density wave instabilities and insulating states. Further, our mean-field slave boson calculations[8] also predict that the insulating state is more stable for $t>0$ than $t<0$, in contrast to the results reported in Fig. 9.

D. Magnetic order

Spin correlations in the model are analyzed through the static spin structure factor

$$S(\mathbf{q}) = \frac{1}{N_s}\sum_{ij} \exp^{i\mathbf{q}\cdot(\mathbf{R_i}-\mathbf{R_j})}\langle S_i^z S_j^z\rangle, \tag{22}$$

where $S_j^z=(n_{j\uparrow}-n_{j\downarrow})/2$ is the z component of the spin at the lattice site $\mathbf{R}_j$.

The dependence on Δ of the spin structure factor, $S(\mathbf{q})$, is shown in Fig. 10 for two different wavevectors with $U=100|t|$. For $t<0$ the results indicate a transition to the magnetically ordered state with wavevector $\mathbf{Q}_1=(\pi,\pi/\sqrt{3})$ (which implies that the spins within the A chains are antiferromagnetically ordered and antiferromagnetically coupled with neighboring A chains) at about $\Delta=2|t|$. This is the spin pattern shown in Fig. 1. For $t>0$ there is a range of Δ for which the A spins are ferromagnetically coupled.

The FM region obtained from Lanczos diagonalization is in agreement with the condition $J<0$ extracted from a strong-coupling expansion. This condition gives a FM region for $5t<\Delta<\sqrt{2}U$.

The wavevector of the magnetic order and the associated magnetic moment of the ground state of the model with $t<0$ and $U\gg\Delta\gg|t|$ (see Fig. 1) are consistent with the antiferromagnetic ordering wavevector observed in $Na_{0.5}CoO_2$.[37,38] However, the observed charge transfer between A and B chains in $Na_{0.5}CoO_2$ [39–41] is much smaller than the complete charge transfer sketched in Fig. 1. Such a large magnetic moment in the presence of a weak charge transfer between A and B sites is not expected from either classical or weak-coupling arguments. Nevertheless, our previous exact diagonalization calculations for $U>W$ (see Fig. 4 of Ref. 7) found a substantial magnetic moment and small charge transfer, even for small Δ, consistent with the experimental results.

IV. DYNAMICAL PROPERTIES

In this section we discuss dynamical properties of the model (1). We use Lanczos diagonalization on $N_s=18$ clusters to compute the one-electron spectral density and the frequency dependent conductivity.

A. One-electron spectral density

The spectral density per spin is

$$A(\omega) = \sum_m |\langle\Psi_m(N-1)|c_{i\sigma}|\Psi_0\rangle|^2\delta\{\omega+[E_m(N-1)-E_0(N)]\} + |\langle\Psi_m(N+1)|c_{i\sigma}^+|\Psi_0\rangle|^2\delta\{\omega-[E_m(N+1)-E_0(N)]\}, \tag{23}$$

where $E_m(N\pm1)$ is the spectra of excitations of the full quantum many-body problem with $N\pm1$ electrons and $|\Psi_m(N\pm1)\rangle$ its associated wave functions. $E_0(N)$ is the ground state of the N electron system with wave function $|\Psi_0\rangle$.

In Fig. 11 we show the spectral density for $U=100|t|$ and

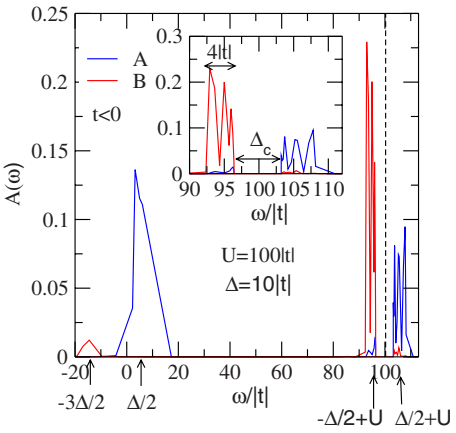

FIG. 11. (Color online) Density of states of the charge-transfer insulator. We take $U=100|t|$, $\Delta=10|t|$, and $t<0$. The inset shows the low-energy part where the charge gap agrees with the strong-coupling expression Eq. (19). The excitation energies in the atomic limit ($t=0$) are shown by the arrows below the abscissa. The chemical-potential ($\omega=\mu$) is shown by the vertical dashed line.

$\Delta=10|t|$. As the system is well into the strong-coupling regime, $U\gg\Delta\gg|t|$, we can understand the main excitations observed on the basis of the atomic limit ($t=0$).

For $t=0$ extracting an electron from the lattice can lead to three possible excitation energies: $-3\Delta/2$, $\Delta/2$, and $-\Delta/2+U$. While adding an electron we only have one excitation energy at $\Delta/2+U$. Therefore, four peaks at these excitation energies are expected in $A(\omega)$. A gap of $\Delta_c=\Delta$ is therefore obtained when $t=0$ typical of a charge-transfer insulator. When the hopping is turned on, the lowest-order correction to excitation energies comes from the propagation of a hole (doublon) along the $B(A)$ chains when extracting (adding) an electron to the zeroth-order ground-state configuration. As the hole (electron) added can be on any site of the chains the ground state is $N_A(N_B)$ *-fold* degenerate. This degeneracy is lifted at the first order in t, where the excitation energies for removing an electron are $\Delta/2-2|t|(\sin(k)-1)$ and $\Delta/2-2|t|\cos(k)$, from the A and B sites, respectively. Adding an electron to the A chain leads to a doublon with excitation energy $\Delta/2+U+2|t|(\sin(k)-1)$ Thus, a characteristic one-dimensional broadening of $4|t|$ to the four peaks should be expected and the gap is reduced from the atomic limit result to $\Delta_c=\Delta-4|t|$. The hybridization between the chains lowers the ground-state energy for the N electron configuration, due to virtual excursions from a B site to a nearest-neighbor A site, by $-4|t|^2/\Delta$ with no cost in Coulomb repulsion energy. Therefore, the lowest $N+1$ electron excitation energy is pushed upwards by $+4|t|^2/\Delta$ and the $N-1$ downward by $-4|t|^2/\Delta$. This leads to an increase in the gap: $\Delta_c=\Delta-4|t|+8t^2/\Delta$. The final charge gap, Δ_c, including the higher-order corrections of Eq. (19) coincides with the numerical calculation shown in the inset of Fig. 11.

In Fig. 12 we show the evolution of $A(\omega)$ with Δ for $U=15|t|$. The four-peak structure discussed above for the CTI remains for this smaller value of U and $\Delta=10|t|$. As Δ decreases the peaks broaden due to hybridization between the A and B chains and shift in energy. For $\Delta=|t|$, $A(\omega)$ contains a lower Hubbard band (LHB), an upper Hubbard

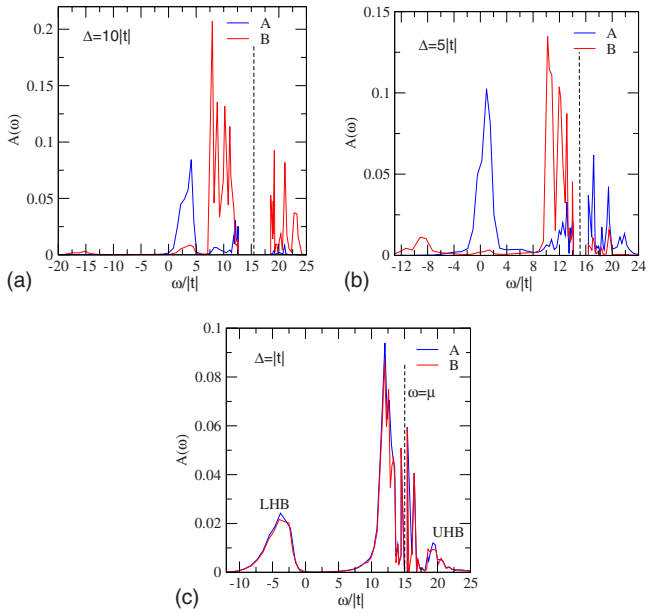

FIG. 12. (Color online) Evolution of the energy dependence of the density of states with decreasing charge transfer. We take $U=15|t|$ and vary Δ from $10|t|$ (top-left, charge-transfer insulator) to $\Delta=|t|$ (bottom, covalent insulator), all with $t<0$. The chemical-potential ($\omega=\mu$) is shown by the vertical dashed lines.

band (UHB) and most of the spectral weight is around the chemical-potential $\omega=\mu$. We find that the energy difference between the LHB and UHB is much larger than U, which we attribute to hybridization between the chains. Thus we identify this regime as a covalent insulator.[7,42]

B. Frequency dependent conductivity

The incoherent part of the optical conductivity is calculated through the current correlation function

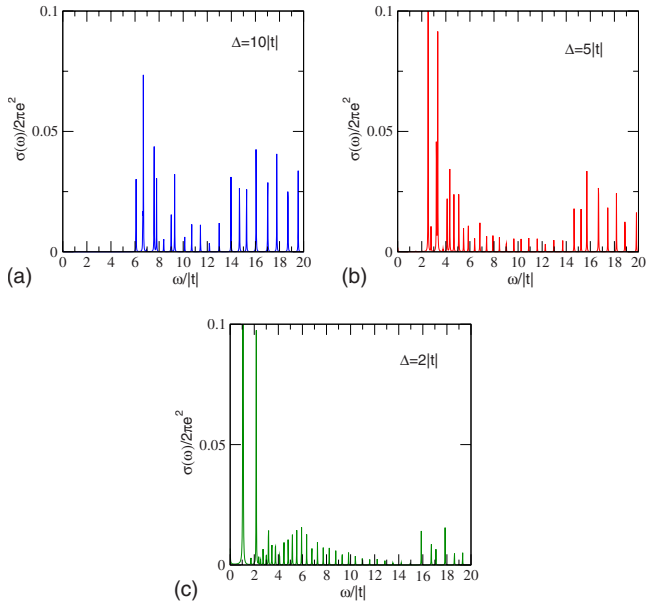

FIG. 13. (Color online) Frequency dependence of the optical conductivity for several values of Δ/t and fixed $U=15|t|$ with $t<0$.

$$\sigma(\omega)=\frac{\pi e^2}{N_s}\sum_{m\neq 0}\frac{|\langle\Psi_m(N)|j_x|\Psi_0\rangle|^2}{E_m-E_0}\delta[\omega-(E_m-E_0)], \tag{24}$$

where, j_x is the x component of the current operator

$$\mathbf{j}=it\sum_{i,\gamma,\sigma}(\mathbf{R}_{i+\gamma}-\mathbf{R}_i)c^+_{i+\gamma,\sigma}c_{i,\sigma}, \tag{25}$$

with $\mathbf{R}_i$ denoting the position of the ith lattice site, and γ its nearest-neighbor sites.

The evolution of the optical conductivity, $\sigma(\omega)$, with Δ is shown in Fig. 13. There are two main absorption bands in the optical spectra. One is fixed at large energies of about U and is associated with excitations between the Hubbard bands and a lower band which shifts with Δ. The lower absorption band is due to excitations associated with transferring an electron from the $-$ band to the $+$ band. These produce a continuum of particle-hole excitations of width of order $W\approx 9|t|$.

We have also calculated the Drude weight for a range of parameters in the model Hamiltonian. We do not show the results here because due to finite-size effects the detailed interpretation is not clear. However, the trend is clear: as $U/|t|$ and $\Delta/|t|$ increase, the Drude weight decreases significantly.

V. CONCLUSIONS

We have considered the electronic properties of an ionic Hubbard model at 3/4-filling with stripes of alternating on-site potential. This model has a rich phase diagram, in which various types of insulating and metallic states compete. A charge-transfer-type insulator, a Mott insulator, and a covalent insulator occur in different $U-\Delta-t$ parameter regimes. The geometrical frustration of the triangular lattice leads to different magnetic properties depending on the sign of t. For $t<0$ an antiferromagnetic interaction occurs whereas for $t>0$ a ferromagnetic coupling occurs in a broad range of parameters.

At $U\gg\Delta\gg|t|$, a charge-transfer insulator of doubly occupied chains of B sites alternating with singly occupied A chains occurs, i.e., $n_B-n_A=1$. As Δ is decreased the system remains insulating although the charge disproportionation between sites is incomplete: $n_B-n_A<1$.

The insulating state of $Na_{0.5}CoO_2$ is characterized by a small charge modulation, a small charge gap, and strong Coulomb interaction. Electronic structure calculations suggest that $Na_{0.5}CoO_2$ is in the parameter regime, $U\gg|t|$ and $\Delta\sim|t|$, which is different to the strong-coupling parameter regime. This regime is difficult to analyze within weak-coupling perturbation theory and numerical approaches are helpful. The model with no charge modulation, $\Delta=0$, reduces to a highly-doped Hubbard (or $t-J$) model on a triangular lattice which is believed to be metallic. However, under a weak external periodic potential, $\Delta\sim O(|t|)$, our exact diagonalization analysis suggests a nonzero charge gap. Unlike the charge-transfer insulators proposed previously for $Na_{0.5}CoO_2$ this insulator is characterized by small real space

charge transfer: $n_B - n_A \ll 1$. An insulating state induced by strong hybridization of the noninteracting bands is realized and is reminiscent of the covalent insulator description of some transition-metal oxides.[42]

The behavior of the charge gap for $U \gg |t|$ has been further explored by an exact analysis of two- and four-site clusters which indicates that the charge gap is always enhanced with Δ even at small values. A different dependence on Δ of the ground state many-body energies $E_0(N)$, $E_0(N-1)$, and $E_0(N+1)$ is found which reflects the different nature of the bonds formed between inequivalent A and B sites. Two-electron bonds are well-described as valence bonds which contain the effects of strong electronic correlations whereas three-electron bonds are accurately described by "molecular" orbitals which are uncorrelated. While the former type of bond depends weakly on Δ the latter does not.

Optical conductivity experiments suggest a gap on the order of 0.020 eV ($\sim|t|/5$), a sharp peak at about 0.026 eV ($\sim|t|/4$), which is at the lower edge of a continuum of excitations which reaches energies up to about 0.9 eV ($\sim 9|t|$).[43] This behavior is consistent with the low-energy adsorption band found in the calculated $\sigma(\omega)$ (see Fig. 13) which is located at about $\Delta \sim O(|t|)$ with the continuum being the whole set of particle-hole excitations between the two hybridized bands which spread over the whole bandwidth $\sim W$.

Recent experiments on Na_xCoO_2 for $x=2/3$ the Na ions induce a charge ordering pattern with filled nonmagnetic Co^{3+} ions arranged in a triangular lattice and $Co^{3.44+}$ magnetic sites forming a kagomé lattice structure with the transferred holes moving on it. These experiments are important as they relate the charge order with the different magnetic and electronic properties of the material. The present ionic Hubbard model modified to include such ordering patterns could be used to explore the unconventional metallic properties of Na_xCoO_2 at $x=2/3$.

We now briefly discuss the relationship between the results we obtained here and those we recently obtained for the same model with a slave boson mean-field theory.[8] Slave bosons give an insulator only for $\Delta > 8|t| (\Delta > 5|t|)$ for $t < 0 (t > 0)$ whereas exact diagonalization suggests that the ground state is insulating even for $\Delta \sim |t|$.

An important open question that this study raises is, what is the ground state for small $\Delta/|t|$? The temperature dependence of the magnetic susceptibility of the $t-J$ model on the triangular lattice has been calculated using exact diagonalization on small clusters.[44] The bottom left panel of Fig. 6 in Ref. 44 shows that for $J=0$ (i.e., $U \to \infty$ in the Hubbard model) that at 3/4-filling that for all temperatures above about $0.4|t|$ that the susceptibility is the same as that for localized noninteracting spin 1/2 particles. The susceptibility has a maximum at about $0.3|t|$ and then decreases with decreasing temperature to a value about two to three times the value for $U=0$. These results raise the question as to the nature of the ground state and the tendency of the electrons to become localized and the spins to antiferromagnetically order, even in the absence of an exchange interaction, due to kinetic antiferromagnetism.[45]

ACKNOWLEDGMENTS

We thank H. Alloul, J. Bobroff, and R.R.P. Singh for helpful discussions. J.M. acknowledges financial support from MICINN (Grant No. CTQ2008-06720-C02-02). B.J.P. was the recipient of Australian Research Council (ARC) Grant No. DP0878523. R.H.M. was the recipient of ARC Grant No. DP0877875. This work was also supported by the ARC Discovery Project Scheme (Projects No. DP0557532 and No. DP0878523). Some of the numerical calculations were performed on the APAC national facility.

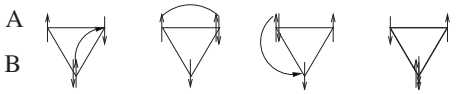

FIG. 14. Three-site "ring" exchange processes contributing to the exchange interaction, J, between neighbor spins in an A chain of the $t-J-J_\perp$ model [compare Eq. (6)].

APPENDIX A: HEISENBERG EXCHANGE COUPLINGS

In this section we discuss the various contributions to the nearest-neighbor exchange coupling, J, between the A sites. Taking $|\Psi_0\rangle$ as the ground-state configuration in the strong-coupling limit $U \gg \Delta \gg t$, there is no correction to the lowest order in the kinetic energy. To $O(t^2)$ we have the usual superexchange antiferromagnetic contribution: $J=4t^2/U$. To $O(t^3)$ "ring" exchange processes around the three-site plaquette of the type shown in Fig. 14 remove the spin degeneracy and were already discussed by Penc and collaborators[23] in a Hubbard model on a zigzag ladder. The energy of the singlet state in Fig. 14 is shifted by $4t^3/\Delta^2$ while the triplet state by $-4t^3/\Delta^2$. These shifts are opposite to the two-site case. As there are two possible ways of going around the triangle in Fig. 14 and there are two neighboring B sites (one below the two A sites as shown in Fig. 14 and another above) the final contribution to the effective J at $O(t^3)$ is $J=E_t-E_s=-8t^3/\Delta^2$ enhancing the ferromagnetic tendencies as compared to the ladder case[23] by a factor of two. In contrast "ring" exchange processes around a four-site plaquette $[O(t^4)]$ of the type shown in Fig. 15 lead to an AF contribution to $J=40t^4/\Delta^3$. Including all possible exchange processes, a total contribution to J valid to $\mathcal{O}((t/\Delta)^4)$ is

$$J = \frac{4t^2}{U} - \frac{8t^3}{\Delta^2} - \frac{16t^3}{\Delta U} + \frac{40t^4}{\Delta^3} + \frac{48t^4}{\Delta^2(2\Delta+U)} + \frac{16t^4}{\Delta^2 U}. \tag{A1}$$

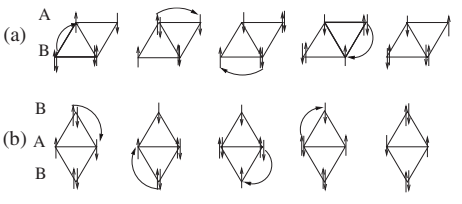

FIG. 15. Four-site "ring" exchange processes of $\mathcal{O}((t/\Delta)^4$ contributing to the exchange interaction between two neighboring sites in the A chains in model (6).

APPENDIX B: GROUND-STATE WAVE FUNCTIONS FOR THE FOUR-SITE CLUSTER AND VALENCE-BOND THEORY

In this appendix, we discuss exact ground-state wave functions on the $N_s=4$ cluster of Fig. 3 with $t'=t$ and $N=5$, 6, and 7 electrons. Valence-bond (VB) states, which are neutral configurations formed by two neighbor electrons in a singlet,[32] are found to describe the exact wave function accurately for $U \gg |t|$ and $t<0$ for $N=6$. This is because ionic configurations have a negligible weight in the full wave function at large U values.

1. Ground state for $N=6$ electrons

The exact ground-state wave function, $|\Psi_0(6)\rangle$, is well-described by the resonance between different possible VB states between electrons inside the cluster

$$|\Psi_0(6)\rangle \approx a\left|\begin{matrix} & \uparrow\downarrow & \\ \uparrow & & \downarrow \\ & \uparrow\downarrow & \end{matrix}\right\rangle + b\left|\begin{matrix} & \uparrow & \\ \uparrow\downarrow & & \uparrow\downarrow \\ & \downarrow & \end{matrix}\right\rangle + c\left(\left|\begin{matrix} & \downarrow & \\ \uparrow\downarrow & & \uparrow \\ & \uparrow\downarrow & \end{matrix}\right\rangle + \left|\begin{matrix} & \downarrow & \\ \uparrow & & \uparrow\downarrow \\ & \uparrow\downarrow & \end{matrix}\right\rangle + \left|\begin{matrix} & \uparrow\downarrow & \\ \uparrow\downarrow & & \uparrow \\ & \downarrow & \end{matrix}\right\rangle + \left|\begin{matrix} & \uparrow\downarrow & \\ \downarrow & & \uparrow\downarrow \\ & \uparrow & \end{matrix}\right\rangle\right). \quad \text{(B1)}$$

Here, singlet VB states are shown as antiparallel spins in boldface. Note that the horizontal sites are A sites while the vertical sites are B sites as sketched in Fig. 3. For $U=\infty$ and $\Delta=0$, the energy of the RVB state is $E_0^{\mathrm{RVB}}(6)=-3.3723|t|$ and the weights of the wave function are $a=b=0.4544$, and $c=0.3831$. This RVB wave function gives an accurate description of the exact ground-state energy which for $U=100|t|$ is: $E_0(6)-2U=-3.453|t|$ and a wave function described by (B1) with $a=0.459$, $b=0.445$, and $c=0.382$, plus small ionic terms. Note that, on the four-site cluster, the A and B sites are not equivalent even for $\Delta=0$ due to geometry of the cluster (cf. Fig. 3).

The RVB wave function also accurately describes the ground-state energy in the limit: $U \gg \Delta \gg |t|$. The energy of the RVB state for $\Delta=10|t|$ is $E_0^{\mathrm{RVB}}=-10.433|t|$, and the wave function has weights $a=0.977$, $b=0.021$, and $c=0.1058$. This is in good agreement with the exact ground state, which has $E_0(6)-2U=-10.453|t|$ and $a=0.976$, $b=0.024$, and $c=0.108$ (plus small ionic terms). Thus, the VB formed between the two A sites dominates the wave function.

2. Ground state for $N=7$ electrons

The seven-electron system contains one hole which can hop around the cluster so the Coulomb interaction has no effect. The ground state is simply a linear combination of the states with one hole in the cluster

$$|\Psi_0(7)\rangle \approx d\left(\left|\begin{matrix} & \downarrow & \\ \uparrow\downarrow & & \uparrow\downarrow \\ & \uparrow\downarrow & \end{matrix}\right\rangle + \left|\begin{matrix} & \uparrow\downarrow & \\ \uparrow\downarrow & & \uparrow\downarrow \\ & \downarrow & \end{matrix}\right\rangle\right) + e\left(\left|\begin{matrix} & \uparrow\downarrow & \\ \uparrow\downarrow & & \downarrow \\ & \uparrow\downarrow & \end{matrix}\right\rangle + \left|\begin{matrix} & \uparrow\downarrow & \\ \downarrow & & \uparrow\downarrow \\ & \uparrow\downarrow & \end{matrix}\right\rangle\right). \quad \text{(B2)}$$

Note that the e and d coefficients are different even for $\Delta=0$ due to the geometry of the cluster (cf. Fig. 3).

3. Ground state for $N=5$ electrons

The five-electron ground-state wave function is approximately described by

$$|\Psi_0(5)\rangle \approx f\left(\left|\begin{matrix} & \downarrow & \\ \uparrow & & \downarrow \\ & \uparrow\downarrow & \end{matrix}\right\rangle + \left|\begin{matrix} & \uparrow\downarrow & \\ \uparrow & & \downarrow \\ & \downarrow & \end{matrix}\right\rangle\right) + g\left(\left|\begin{matrix} & \downarrow & \\ \uparrow\downarrow & & \uparrow \\ & \downarrow & \end{matrix}\right\rangle + \left|\begin{matrix} & \downarrow & \\ \uparrow & & \uparrow\downarrow \\ & \downarrow & \end{matrix}\right\rangle\right). \quad \text{(B3)}$$

This state with two spin-up electrons and three spin-down electrons have $S^z_{tot}=-1/2$ which is degenerate to the $S^z_{tot}=+1/2$ (not shown). In the first configuration two spins on the A sites combine into a singlet whereas in the last configuration a triplet between B sites is formed (the parallel spins in boldface denote the triplet combination). Hence, for this case, ferromagnetic correlations occur between B sites in contrast to the antiferromagnetic correlations between electrons on the A sites. For $U=100|t|$ and $\Delta=0$, the ground-state energy: $E_0(5)-U=-2.41|t|$. while for $\Delta=10|t|$ the ground-state energy is $E_0(5)-U=-5.385|t|$.

[1] P. A. Lee, Rep. Prog. Phys. **71**, 012501 (2008).

[2] T. Ishiguro, K. Yamaji, and G. Saito, *Organic Superconductors*, 2nd ed. (Springer, New York, 2001); B. J. Powell and R. H. McKenzie, J. Phys.: Condens. Matter **18**, R827 (2006).

[3] M. B. Salamon and M. Jaime, Rev. Mod. Phys. **73**, 583 (2001).

[4] P. Gegenwart, Q. Si, and F. Steglich, Nat. Phys. **4**, 186 (2008).

[5] M. R. Norman, Phys. **1**, 21 (2008); W. E. Pickett, Nat. Phys. **5**, 87 (2009).

[6] J. Merino, B. J. Powell, and R. H. McKenzie, Phys. Rev. B **73**, 235107 (2006).

[7] J. Merino, B. J. Powell, and R. H. McKenzie, Phys. Rev. B **79**, 161103(R) (2009).

[8] F. Litaiff, J. R. de Sousa, and N. S. Branco, Solid State Commun. **147**, 494 (2008).

[9] M. Roger, D. J. P. Morris, D. A. Tennant, M. J. Gutmann, J. P. Goff, J. U. Hoffmann, R. Feyerherm, E. Dudzik, D. Prabhaka-

ran, A. T. Boothroyd, N. Shannon, B. Lake, and P. P. Deen, Nature (London) **445**, 631 (2007).
[10] P. Zhang, R. B. Capaz, M. L. Cohen, and S. G. Louie, Phys. Rev. B **71**, 153102 (2005).
[11] T. Egami, S. Ishihara, and M. Tachiki, Science **261**, 1307 (1993).
[12] N. Nagaosa and J. Takimoto, J. Phys. Soc. Jpn. **55**, 2735 (1986); **55**, 2745 (1986); N. Nagaosa, *ibid.* **55**, 2754 (1986).
[13] H. Yoshioka, H. Seo, and H. Fukuyama, J. Phys. Soc. Jpn. **74**, 1922 (2005).
[14] S. Okamoto and A. J. Millis, Phys. Rev. B **70**, 075101 (2004).
[15] S. Ishihara, T. Egami, and M. Tachiki, Phys. Rev. B **49**, 8944 (1994).
[16] A. P. Kampf, M. Sekania, G. I. Japaridze, and Ph. Brune, J. Phys.: Condens. Matter **15**, 5895 (2003), also see references therein and citations thereof for further details of the extensive literature on the ionic Hubbard model in one dimension.
[17] G. I. Japaridze, R. Hayn, P. Lombardo, and E. Müller-Hartmann, Phys. Rev. B **75**, 245122 (2007).
[18] A. Garg, H. R. Krishnamurthy, and M. Randeria, Phys. Rev. Lett. **97**, 046403 (2006).
[19] L. Craco, P. Lombardo, R. Hayn, G. I. Japaridze, and E. Müller-Hartmann, Phys. Rev. B **78**, 075121 (2008).
[20] S. S. Kancharla and E. Dagotto, Phys. Rev. Lett. **98**, 016402 (2007).
[21] N. Paris, K. Bouadim, F. Hebert, G. G. Batrouni, and R. T. Scalettar, Phys. Rev. Lett. **98**, 046403 (2007).
[22] K. Bouadim, N. Paris, F. Hébert, G. G. Batrouni, and R. T. Scalettar, Phys. Rev. B **76**, 085112 (2007).
[23] K. Penc, H. Shiba, F. Mila, and T. Tsukagoshi, Phys. Rev. B **54**, 4056 (1996).
[24] M. S. Laad, L. Craco, and E. Müller-Hartmann, Phys. Rev. B **64**, 195114 (2001).
[25] K. Byczuk, W. Hofstetter, and D. Vollhardt, Phys. Rev. B **69**, 045112 (2004).
[26] K. Byczuk, M. Ulmke, and D. Vollhardt, Phys. Rev. Lett. **90**, 196403 (2003).
[27] C. A. Marianetti and G. Kotliar, Phys. Rev. Lett. **98**, 176405 (2007).
[28] M. L. Foo, Y. Wang, S. Watauchi, H. W. Zandbergen, T. He, R. J. Cava, and N. P. Ong, Phys. Rev. Lett. **92**, 247001 (2004).
[29] H. W. Zandbergen, M. L. Foo, Q. Xu, V. Kumar, and R. J. Cava, Phys. Rev. B **70**, 024101 (2004).
[30] G. León, C. Berthod, T. Giamarchi, and A. J. Millis, Phys. Rev. B **78**, 085105 (2008); G. León, Ph.D. thesis, University of Geneve, 2008.
[31] C. Weber, A. Läeuchli, F. Mila, and T. Giamarchi, Phys. Rev. B **73**, 014519 (2006).
[32] L. Pauling and E. B. Wilson, Jr., *Introduction to Quantum Mechanics with Applications to Chemistry* (Dover, New York, 1985); F. Wienhold and C. Landis, *Valency and Bonding* (Cambridge University Press, Cambridge, England, 2005).
[33] M. Ogata and H. Shiba, Phys. Rev. B **41**, 2326 (1990).
[34] L. Balicas, M. Abdel-Jawad, N. E. Hussey, F. C. Chou, and P. A. Lee, Phys. Rev. Lett. **94**, 236402 (2005).
[35] D. Qian, L. Wray, D. Hsieh, D. Wu, J. L. Luo, N. L. Wang, A. Kuprin, A. Fedorov, R. J. Cava, L. Viciu, and M. Z. Hasan, Phys. Rev. Lett. **96**, 046407 (2006).
[36] M. Getzlaff, *Fundamentals of Magnetism* (Springer, New York, 2007), p. 62.
[37] G. Gasparovic, R. A. Ott, J.-H. Cho, F. C. Chou, Y. Chu, J. W. Lynn, and Y. S. Lee, Phys. Rev. Lett. **96**, 046403 (2006).
[38] H. Watanabe, Y. Mori, M. Yokoi, T. Moyoshi, M. Soda, Y. Yasui, Y. Kobayashi, M. Sato, N. Igawa, and K. Kakurai, J. Phys. Soc. Jpn. **75**, 034716 (2006).
[39] J. Bobroff, G. Lang, H. Alloul, N. Blanchard, and G. Collin, Phys. Rev. Lett. **96**, 107201 (2006).
[40] A. J. Williams, J. P. Attfield, M. L. Foo, L. Viciu, and R. J. Cava, Phys. Rev. B **73**, 134401 (2006).
[41] D. N. Argyriou, O. Prokhnenko, K. Kiefer, and C. J. Milne, Phys. Rev. B **76**, 134506 (2007).
[42] D. D. Sarma, J. Solid State Chem. **88**, 45 (1990); T. Mizokawa, A. Fujimori, H. Namatame, K. Akeyama, and N. Kosugi, Phys. Rev. B **49**, 7193 (1994).
[43] N. L. Wang, G. Li Dong Wu, X. H. Chen, C. H. Wang, and X. G. Luo, Phys. Rev. Lett. **93**, 147403 (2004); J. Hwang, J. Yang, T. Timusk, and F. C. Chou, Phys. Rev. B **72**, 024549 (2005); S. Lupi, M. Ortolani, L. Baldassarre, P. Calvani, D. Prabhakaran, and A. T. Boothroyd, *ibid.* **72**, 024550 (2005).
[44] J. O. Haerter, M. R. Peterson, and B. S. Shastry, Phys. Rev. B **74**, 245118 (2006).
[45] J. O. Haerter and B. S. Shastry, Phys. Rev. Lett. **95**, 087202 (2005).